IEEE Access
Multidisciplinary | Rapid Review | Open Access Journal

Received 28 September 2022, accepted 11 October 2022, date of publication 13 October 2022, date of current version 19 October 2022.

Digital Object Identifier 10.1109/ACCESS.2022.3214651

RESEARCH ARTICLE

Copper Pipes as Medium Frequency Transformer Windings

NIKOLINA DJEKANOVIC, (Graduate Student Member, IEEE), AND DRAZEN DUJIC, (Senior Member, IEEE)

Power Electronics Laboratory, École Polytechnique Fédérale de Lausanne (EPFL), 1015 Lausanne, Switzerland

Corresponding author: Nikolina Djekanovic (nikolina.djekanovic@epfl.ch)

The results presented in this paper are a part of the EMPOWER project that has received funding from the European Research Council (ERC) under the European Union's Horizon 2020 research and innovation programme (Grant agreement No. 818706).

ABSTRACT Owing to increasing power demand, new technologies, such as solid-state transformers, are progressively researched and improved. Thereby, galvanic isolation and voltage adaptation are achieved by medium frequency transformers. To reach high power density designs, transformer windings can be realized by means of copper pipes, allowing for efficient liquid cooling. This paper provides insight to many relevant aspects for the use of hollow copper conductors as windings. This includes electrical and thermal modeling, as well as considerations regarding mechanical implementations. Additionally, the winding concept is investigated based on a 1 MW medium frequency transformer prototype.

INDEX TERMS Medium-frequency transformer windings, hollow conductors, internal water cooling, oil insulation.

I. INTRODUCTION

The global power demand is constantly increasing. This results in growing power ratings of converter systems, which further calls for increased efficiencies and higher power densities in many applications. Technologies, such as the solid-state transformers (SSTs), offer higher flexibility and advanced conversion concepts, and are thus being considered in various contexts with applications that involve medium voltage (MV) to low voltage (LV) power conversion. Some of the examples include providing the necessary link between distribution grids on one side and energy storages and renewable energy sources on the other side, traction applications [1], [2], and marine on-board power distribution networks [3], [4].

Medium frequency transformer (MFT) constitutes an integral part of every SST, since it realizes galvanic isolation and voltage adaptation between the power stages. A standard winding technology for majority of MFTs is to use litz wires, aiming to reduce the eddy current effects and thus the losses during operation at elevated frequencies. Yet, to minimize the loss, the number of fine strands in a litz wire generally needs to be set very high. This in turn leads to increased expenses/costs and to a lower packing factor, due to enlarged space for strand insulation [5]. Therefore, it is worth looking into alternatives for MFT windings in high power applications. Assuming constant efficiency of power stages, semiconductor losses are proportionally increasing, relative to the overall converter ratings. Considering high power MV converters, cooling systems based on natural or forced air convection become insufficient and replaced with more efficient liquid cooling solutions. In the case of water as a cooling medium, it manifests both higher specific heat capacity and thermal conductivity in comparison to air. Due to the fact that the circulating cooling medium is in contact with components/heatsinks at various MV potentials, it is important to ensure its low electrical conductivity. This is typically achieved with deionized (DI) water [6], [7]. Finally, having actively cooled power stages supports and encourages the use of hollow conductors as MFT windings.

Copper tubes have been actively employed world-wide since the 1930s primarily for hot and cold water systems. This includes applications such as plumbing, heating, air conditioning and refrigeration. Recently, they have found

The associate editor coordinating the review of this manuscript and approving it for publication was Javier Moreno-Valenzuela.

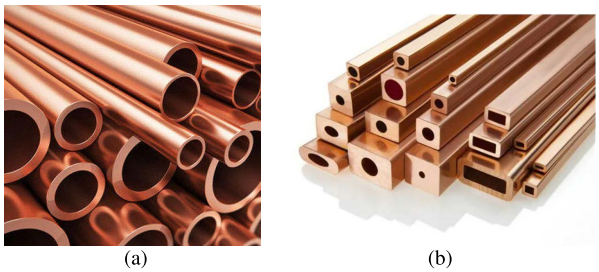

(a) (b)

FIGURE 1. (a) Pipes [8] and (b) tubes [9] made of copper.

increased use in natural and medical gas systems as well [10]. However, the focus of the above mentioned applications lies in the capability of copper to conduct heat. That being said, this paper looks into copper tubes which are primarily used as electrical conductors with an open possibility of internal cooling.

Some of the properties that speak for the wide range of copper tube usage is the material's lightweight, high mechanical strength, high corrosion resistance, as well as availability in various lengths, diameters and wall thicknesses [11]. Consequently, copper tubes are able to meet the needs of a broad spectrum of conditions and applications, and additionally they are cost-effective. Moreover, copper is available in various tempers, which is a measure of its hardness and strength, going from drawn (hard) to annealed (soft) copper.

A typical electrical application of copper hollow conductors is as stator windings of electrical machines, commonly operated in the generator mode. Such generators can be found in various range of applications, from aircrafts, where the coolant is the phase change material [12], [13], pumped-storages and nuclear power plants [14], [15], [16], to evaporative cooling hydrogenerators of several hundreds of MWs of nominal power [17], [18]. This testifies about the advantages of using tubes as conductors, especially having in mind the increased power density. In the recent years, the use of copper pipes as windings has been additionally aided by additive manufacturing, which opened up a variety of geometries to designers of electrical machines in particular [12].

Note that today the terms pipe and tube are used interchangeably, however, there are several distinctions between them. Namely, the main differences are in regards to applications, typical size characteristic and the shape, as can be seen in Fig. 1. Pipes have only round cross sections, whereas tubes can have round, square, rectangular and oval hollow sections. In addition, tubes are used for structural purposes (to provide mechanical support) and the important characteristic is the outer diameter (OD) and the wall thickness. In the case of pipes, they are commonly used for transporting of gasses and liquids, as vessels, and therefore, it is important to know the pipe's capacity, i.e. inner diameter (ID). Alike pipes, tubes follow and respect tighter tolerances. For the application that is considered in this paper, the term pipes will be used, since the work is limited to round hollow conductors. Nevertheless, both ID and OD dimensions of the pipe are equally important for the winding design. The difference of OD and ID defines the wall thickness of the pipe, which is relevant for the skin effect considerations due to high operating frequencies.

When it comes to employment of hollow conductors as transformer windings, there are not many published results in the literature that cover high power, medium frequency and medium voltage domain, compared to other more common conductors (foil, litz wire and so on). The 166 kW MFT presented in [19] and a 350 kW MFT from [20] both use rectangular aluminum profiled tubes for current conduction and DI water as the cooling medium. Moreover, when coaxial conductors are used as transformer windings, the inner conductor can be internally cooled, as demonstrated in [21] and [22]. The same principle is applied as for the hollow conductors, yet, the construction of such conductors is significantly more complex [22].

A striking difference between the above-mentioned MFT examples and the topic of this paper is in the selected conductor material. From the physics' aspect aluminum is significantly (around 40%) less conductive than copper, yet, it weighs only 30% of the weight of copper. Ultimately, the selection boils down to the application specific drivers and the targeted cost and power density. Considering that both MFTs [19], [20] are intended for traction applications, where weight and space are limited, aluminum hollow conductors likely make a better choice. Conversely, for the considered application of the presented work, which is MVDC power distribution networks or utility stationary equipment, the emphasis is put on achieving high efficiency over power density.

Main contributions of the paper are given in the following. It elaborates challenges of using copper pipes as transformer windings in MV high power applications, due to the open possibility for very efficient liquid cooling by using the inner pipe channel. The paper provides insight into the essential models necessary to evaluate and characterize copper pipes as windings in a design optimization tool of a high power MFT. Particular focus is set on the thermal modelling of windings in combination with DI water cooling and oil insulation. Lastly, mechanical considerations and challenges about the implementation and realization of pipe windings are included, so that future MFT designers are aware of all the strong and weak aspects of this conductor type.

This paper is organized as follows: Section II introduces the case study example of a high power MFT that uses copper pipes as winding technology. Section III provides deeper insight about copper properties and particularities regarding practical implementations of pipes. The following section deals with modeling of characteristic inductances, whereas Section V discusses modeling of conduction losses for this type of conductors. Section VI gives information about thermal modeling. In Section VII the 1 MW MFT prototype is introduced. Finally, Section VIII provides the overall conclusions.

II. 1 MW, 5 kHz MFT DESIGN

The MFT which is selected as the case study example of copper pipe windings is envisioned as an integral part of a

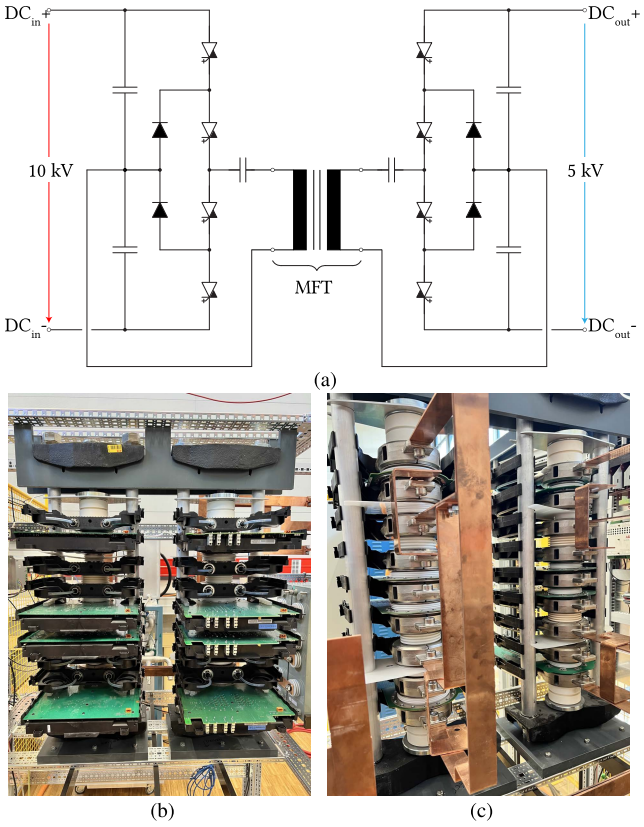

FIGURE 2. (a) DC transformer with 3-level NPC power stages. Reverse conducting IGCTs are used, and rated at 10 kV (engineering samples) and 4.5 kV for the primary and secondary converter side, respectively. (b) and (c) show IGCT stacks used for the two power stages of the 1 MW DCT demonstrator.

1 MW rated DC transformer (DCT). The DCT is proposed as a DC-DC converter utilizing the resonant conversion principle and integrated gate-commutated thyristors (IGCTs) as high-voltage switching devices [23]. The electrical schematic is shown in Fig. 2a, together with DI water cooled IGCT stacks used for the power stages, shown in Fig. 2b and 2c. The selection of the semiconductor device resulted in upper limit of 5 kHz for the operating frequency [24]. The inverter and the rectifier bridge, interconnected with the MFT and the resonant capacitors, are using the 3-level neutral point clamped (NPC) topology.

The electrical MFT requirements are derived from the design specifications of the DCT and are outlined in Table 1 [25]. As can be seen, the operating frequency is set to 5 kHz, as a result of design optimization work that is not presented here. The primary winding (PW) voltage of the analyzed MFT is rated to ±5 kV, the secondary winding (SW) voltage to ±2.5 kV. For the DCT the LLC topology is selected from the family of resonant topologies, which directly implies that the magnetizing and the leakage inductance of the MFT constitute the resonant tank, together with external resonant capacitors. Due to this fact and for flexibility reasons a wider target range is selected for the two characteristic MFT inductances, stated in Table 1.

TABLE 1. MFT electrical requirements.

Characteristics	Unit	Value
Frequency	kHz	5
Nominal power	MW	1
Turns ratio	1	2 : 1
Primary voltage	kV	±5
Secondary voltage	kV	±2.5
Reference magnetizing inductance	mH	25 – 40
Reference leakage inductance	µH	25 – 50

Fig. 3 illustrates the core-type 2-vessel MFT concept which includes a core made of nanocrystalline and two oil vessels, placed around each of the core limbs. Each vessel holds a layer of PW, which encircles a layer of SW. As discussed throughout the paper, the transformer windings are realized in the form of copper pipes with round cross section profile, which allows for internal DI water cooling. To optimally use the space in the vessels and to ensure transformer symmetries, which generally simplifies modeling of relevant phenomenon, conductors with the same cross section profile were selected for both PW and SW. In each vessel both windings have the same number of turns, i.e. they occupy the same vertical height. The required turns ratio is achieved by externally connecting the PWs from the two vessels in series, and the SWs in parallel. Nevertheless, such winding arrangement implies equal current densities in all the windings, considering that for 2:1 turns ratio the SW carries double the current compared to the PW side current. For the presented design, the current density reaches approximately 6 A mm^{-2} for the nominal operating point.

Furthermore, the MFT is connected to the water cooling unit (WCU) in the way that the DI water of lower temperature, compared to the average temperature of the conductors, enters the windings at the top inlet of each vessel

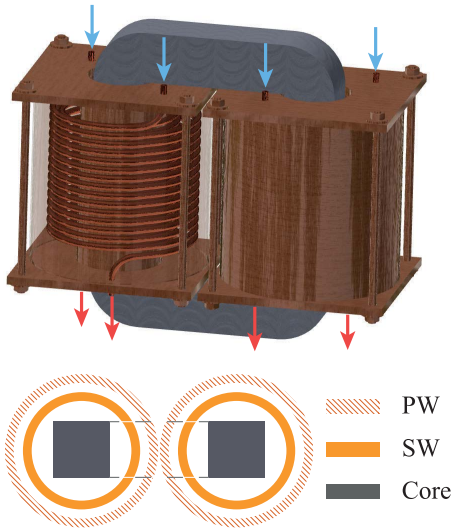

FIGURE 3. 2-vessel MFT design concept with the corresponding top cross section view.

TABLE 2. Copper skin depths at various frequencies.

f (kHz)	≤1	3	5	7	9	10	≥50
δ (mm)	≥2.06	1.19	0.92	0.78	0.69	0.65	≤0.29

(marked with blue arrows in Fig. 3) and exits heated at the bottom outlet (marked with red arrows). Finally, the MFT design optimization tool requires reliable models for conduction losses, leakage inductance, pressure drop, thermal characterization of round hollow conductors. All the relevant models are explained in more details in the remainder of the paper, the main challenges are addressed and resolved.

III. MECHANICAL CONSIDERATIONS

For applications that require high thermal or electric conductivity, copper is mostly used in its pure state. On the other hand, by creating alloys, the most known are bronze and brass, certain copper properties, like corrosion and wear resistance can be improved. Corrosion resistance property of copper lies in the ability of the material to form a uniform and protective oxide layer in contact with most water types. Nevertheless, situations exist where the protective film does not form properly and various types of corrosion may occur [26]. In this work such effects are not considered and it is assumed that no corrosion happens inside of the copper pipes.

The following sections deal with practical limitations and provide guidelines for selecting appropriate pipes for the task of transformer windings.

A. IMPLEMENTATION CHALLENGES

An important thing to have in mind from electrical point of view when using copper pipes as transformer windings is the wall thickness. Depending on the operating frequency of the MFT, the skin effect, which decreases the effective cross section area of the conductor, thus increasing the resistance, can be more or less pronounced. It is characterized by the skin depth which is determined by the following equation [27]

$$\delta_{\mathrm{Cu}}(f) = \sqrt{\frac{\rho}{\pi f \mu_{\mathrm{r,Cu}} \mu_0}}, \quad \text{with} \quad \mu_{\mathrm{r,Cu}} \approx 1. \tag{1}$$

It depends on the material properties such as specific resistance (ρ) and relative permeability ($\mu_{\mathrm{r,Cu}}$). The factor μ_0 is the vacuum permeability. Table 2 gives information about skin depth values in the range of 1 kHz to 50 kHz. As visible from (1), the skin depth decreases inverse proportionally with a square root of the frequency.

In the existing literature on pipes as transformer windings the wall thickness was set to the skin depth of the nominal operating frequency. In this paper, this is adopted as one of the design rules, since in this way the skin effect can be mitigated. Nevertheless, due to manufacturing limits this cannot be respected for an arbitrary frequency, since according to Industry Standard Guide [28] when it comes to standard copper pipes, the lowest wall thickness of Type M designated by ASTM standard is approximately 0.6 mm. Of course, the authors do not exclude the option of custom pipe manufacturing with walls thinner than smallest standard pipe. Therefore, a conclusion can be made that in order to follow the design rule for minimal conduction losses, i.e. to set the wall thickness equal to the skin depth, pipes as windings could be used for MFT designs up to 10 kHz. Fig. 4 shows a typical chart containing manufacturing pipe limits considering the outer diameter and the wall thickness, provided by [9]. For MV high power MFTs the region 2 provides a suitable range of solutions in regards to wall thickness - OD relation.

According to [29] and depending on the bend radius, there are three fundamental approaches to pipe bending. Namely, compression, draw (mandrel) and roll bending. The compression bending applies to the use of manual pipe bending tools or manual bending for small diameters. In the case of mandrel bending, which is used for stiffer materials and pipes of larger diameters, the use of winding machine is essential. There, the pipe is pulled or drawn around the former tool, i.e. mandrel. Lastly, roll bending is used when large radius of curvature is desired and it is usually achieved with three rollers. For the application that is considered in this paper, the second method is considered to be most suitable and it is described in more detail in Section II. As for the size of the bending radius, a standard recommended by [29] is 2OD, i.e. twice the size of the OD of the pipe, measured to the center line. An additional remark is given that the draw bending radius can be as low as $\frac{1}{2}$OD, which depends on the shape, size and cost of the tool. On the other hand, pipe manufacturer Luvata [9] recommends respecting at least 3OD for the bend radius. As for the direction of pipe winding, this can be performed counterclockwise, i.e. regarding the left chirality, or in the clockwise direction, regarding the right chirality. The direction itself does not have an influence on the difficulty/complexity of the winding process.

So far, circular shapes of MFT windings were discussed. This is due to the fact that the core cross section was assumed to be square and the fact that pipes with round cross sections were considered. Nevertheless, high power transformers require bigger cross sectional areas with dimensions that can easily reach limits in core manufacturing. Solution to the

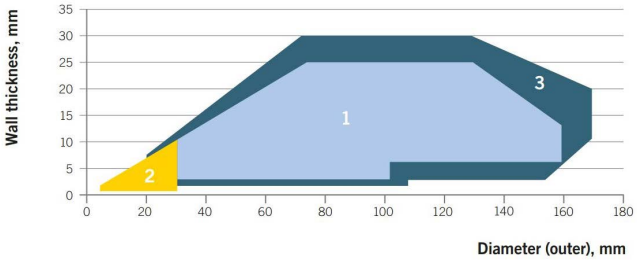

FIGURE 4. Mechanical limits of copper pipes manufacturing by Luvata [9]. Region 1 is for tubes in straight length, region 2 for tubes in coil, region 3 are dimensions available upon request.

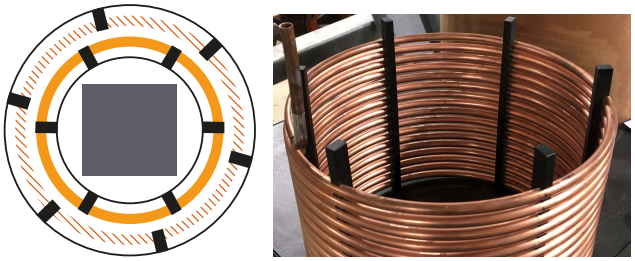

FIGURE 5. (a) Arrangement of spacers for PW and SW; (b) Comb-alike spacers mounted at every 60° on the SW from the inside.

problem lies in having a rectangular core cross section. This is additionally discussed in Section III-B.

Once the windings are brought to the correct shape, the next challenge is to keep the structure compact and in fixed position regarding other windings, or the oil vessel, as it is the case for the MFT presented in the previous section. There are many ways how this can be done with more or less material, using a more or less complex solution. The authors wanted to minimize the size and volume of the supporting system, further referred to as spacer, but maintain the functionality, since it represents an obstacle to the moving insulation fluid. Moreover, a suitable material needs to be selected considering the medium the windings are set in, i.e. material's oil compatibility and considering high temperatures both windings and oil can reach during operation.

As a viable solution six comb-alike structures are added to both PW and SW, made of thermoplastic material POM which complies well with the described requirements. Fig. 5a gives the top cross-sectional view of one of the oil vessels, with the core limb in the inner tube, and describes the position of the 12 spacers. Note that for the PW the spacers are placed from the outside in order to keep fixed distance to the vessel's outer wall. Accordingly, for the SW they are attached from the inner side. In this way the spacers ensure concentricity of the windings, since both outer and inner vessel walls can be considered perfectly circular. Fig. 5b shows the SW with the mounted spacers. Apart from providing compactness and correct distancing to the vessel walls, the supporting structure keeps a fixed turn-to-turn distance, which is essential for correct insulation. Several examples of practical implementations are given in Fig. 6. Note that the spacers could additionally serve as clamping mechanism to prevent mechanical damages in case high electromagnetic forces are exerted onto the windings, in case of fault conditions. To achieve this second functionality, maximum axial and radial forces have to be accurately estimated in various fault settings and the selected set of spacers needs to be able to withstand the applied forces. Detailed explanations concerning this point are provided in Section III-C.

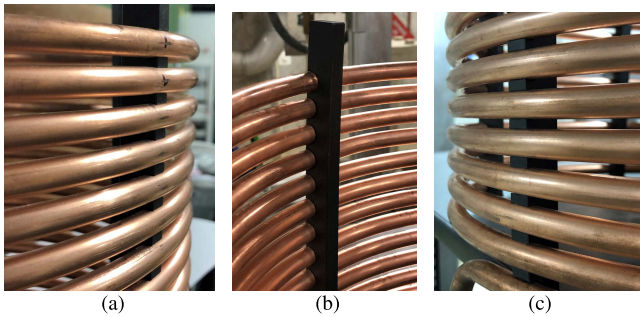

FIGURE 6. Examples of comb-alike spacers mounted at various places from the inner side of the SW.

Regarding the turn-to-turn distance, this value depends on the dielectric properties of the insulation liquid, on the voltage applied to the considered winding and the respective number of turns. The logic behind it follows a simple calculation presented in the following example. Consider a winding with $N_w = 10$ turns immersed in oil with an average value of $E_d = 40\,\text{kV mm}^{-1}$ of dielectric strength. The winding test voltage is set to $V_w = 25\,\text{kV}$, which further implies that $V_{tt} = \frac{V_w}{N_w} = 2.5\,\text{kV}$ needs to be blocked between each of the turns. The required insulation distance between two turns is finally calculated by the following $v_d = \frac{V_{tt}}{E_d} = 62.5\,\mu\text{m}$. However, when choosing the optimal turn-to-turn distance in practice several things need to be kept in mind. Namely, regardless of the fact that soft temper copper is used, non-idealities occur in the winding process, i.e. the turns are not perfectly circular and the winding is prone to mechanical deformations during the manipulation process. Furthermore, oil as insulation fluid exhibits higher viscosity compared to e.g. water, which implies that oil needs a minimal amount of space between two turns to reach all the copper areas. According to industrial experience, the turn-to-turn distances are enlarged to 2−3 mm, which significantly increases the dielectric withstand needs.

Additional attention needs to be paid to terminations of copper pipes, since it is necessary to separate the cooling, i.e. DI water from the electrical connection. There are many ways to achieve an electrical connection, such as soldering or brazing a contact directly at the pipe's end, or adding a removable copper connector to interface the pipe and the rest of the system. On the other hand, the cooling medium is usually conveyed with the help of a plastic pipe of appropriate OD, by an overlap joint or through an adequate connector to make a direct connection between two pipes.

Due to presence of oil, it is required to make a leak-proof, i.e. sealed exit of both windings at the top and bottom of each vessel. For this purpose, a brass pipe fitting of the appropriate ID, with a fixed jam nut and a seal rubber, is brazed at top and bottom of each winding termination, as shown in Fig. 7a. After the vessel is closed, by adding another jam nut from the outer side a sealed connection can be made. Fully sealed connection is shown in Fig. 7b. Additionally, a plastic hose is attached to the pipe, secured with a clamp, to establish a cooling connection with the WCU. The electrical connection between the pipes, i.e. MFT windings and the surrounding power stages is made by clamp-alike copper connectors, with

FIGURE 7. (a) Brass pipe fitting used to ensure a sealed exit of the winding through the vessel lid; (b) Implementation of electrical and cooling connections between a pipe winding end and the rest of the system.

appropriate cable lug endings to accommodate cable connection to the power stages, as shown in Fig. 7b.

Lastly, one can imagine a hypothetical scenario where each vessel contains m PW layers and n SW layers, as illustrated in Fig. 8. Additionally, it is assumed that the windings are interleaved, in order to minimize the conduction losses, as well as the leakage inductance. In the case of litz wires, the winding process would not be disadvantaged by the increase of layer number, but it would require a more complex coil former. On the other hand, continuous winding of several layers for copper pipe PW and SW, with different external radii for every layer, poses a mechanical challenge. To be able to achieve it, mandrels of different sizes are necessary, or a more complex solution of a single mandrel with adjustable external diameter. Alternatively, the necessary electrical connections between the layers can be done externally, which requires each winding layer to exit the vessel and electrically connect to the following layer outside of the vessel. Besides increased complexity, this alternative implies increased winding resistance and ultimately higher winding losses.

For simplicity reasons and to avoid dealing with such problems, the winding design selected for the MFT prototype considers having a single layer of PW and a single layer of SW in each of the vessels. Eventually, the required turns ratio from Table 1 is achieved by an external connection of the corresponding windings from the two oil vessels.

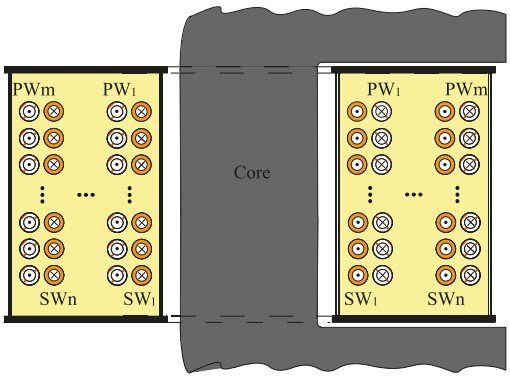

FIGURE 8. Multiple PW and SW layers in a single oil vessel with specified current direction. Without loss of generality, it is assumed that the turns number in each layer is the same, and that the same copper pipes are used for all the windings.

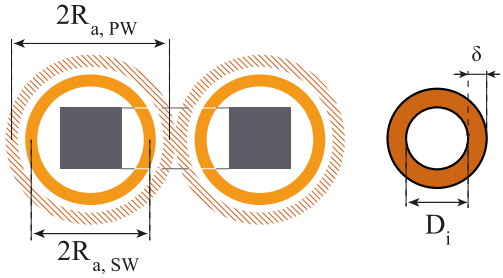

FIGURE 9. Characteristic sizes of the pipes used as primary and secondary winding.

B. COPPER PIPES SELECTION

The key properties used to describe any circular pipe winding include the inner diameter (D_i), the wall thickness of the conductor's cross section (δ), and the external radius of the windings (R_a). Note that R_a corresponds to the half distance between the center lines of the pipes as indicated in Fig. 9, together with other quantities.

The total length of the winding (l) is determined by the number of turns (N) and the distance between each of the turns (v_d), and it is given in the following relation:

$$l = 2\pi N \sqrt{R_\mathrm{a}^2 + \left(\frac{v_\mathrm{d} + D_\mathrm{i} + 2\delta}{2\pi}\right)^2} \tag{2}$$

Note that the derived length only applies to the N turns of the winding, i.e. the additional termination pipe length is not included. Other derived winding properties, such as the conduction losses and the pressure drop along the winding's length, depend on the operating point of the transformer.

An important design aspect when using copper pipes as windings in combination with cooling coordination is the pressure loss along the pipe due to the passing fluid. Depending on the WCU which is used, there is a limit regarding cooling capacity, volumetric flow and allowed pressure drop. To be able to estimate the pressure loss, an empirical equation is used, known as Darcy-Weisbach equation [30]. It quantifies pressure drop due to friction along a pipe of certain geometry, depending on the average velocity of the passing fluid and the type of flow. It is given by the following relation

$$\Delta p = l f_\mathrm{D} \frac{\rho}{2} \frac{\langle v \rangle^2}{D_\mathrm{i}}, \quad \text{with } f_\mathrm{D} = \frac{64}{\mathrm{Re}} \text{ and } \mathrm{Re} = \langle v \rangle \frac{D_\mathrm{i}}{\nu}. \tag{3}$$

The parameter l gives the pipe length, as defined in (2), f_D is the Darcy friction factor, Re is the Reynolds number, $\langle v \rangle$ is the average coolant velocity, whereas ν is its kinetic viscosity and ρ its density. It is assumed that the coolant is moving in a laminar way, which implies the Reynolds number needs to have a value below 2000, empirically determined [31]. The average velocity is determined by the ratio of the average

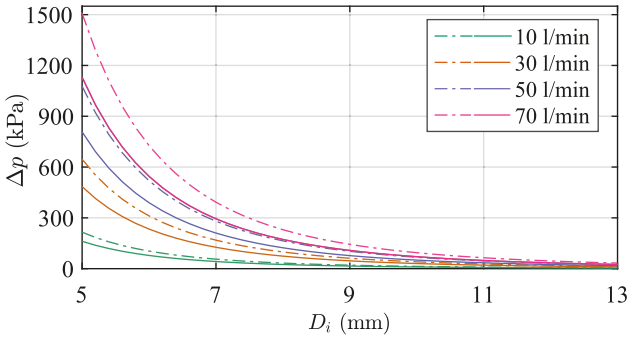

FIGURE 10. Pressure drop along the pipe winding versus inner diameter for various volumetric flows, reaching from 10 l/min to 70 l/min and for two different pipe lengths, 15 m presented by a solid and 20 m by a dashed line.

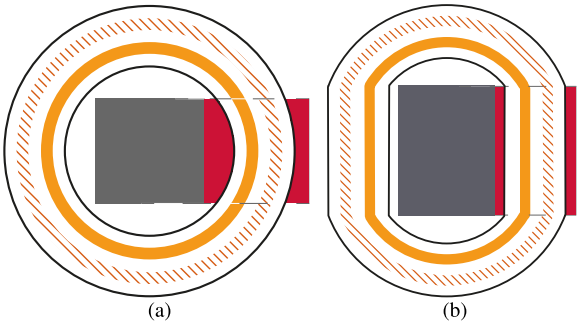

FIGURE 12. (a) Square and (b) rectangular core cross section area with half window area marked with grey dashed lines. The red surfaces mark the lost core window area due to necessary space for the winding turn and the vessel to vessel distance in the case of 2-vessel MFT structure.

volumetric flow Q and the cross section of the wetted area A_w, which is directly proportional to the inner pipe diameter. Considered together with (3), this further implies

$$\Delta p = 128\, l \rho \nu \frac{Q}{D_i^4 \pi}, \quad \text{with} \quad \langle v \rangle = \frac{Q}{A_w} = \frac{4Q}{D_i^2 \pi}. \tag{4}$$

As can be concluded, the pressure drop is heavily influenced by the inner diameter value. In addition, this is illustrated in Fig. 10. It can be noticed that for increased values of inner diameter, starting from $\approx$ 8 mm the pressure drop is less sensitive to the change of pipe length or the flow intensity.

Another quantity describing a certain transformer design is the fill factor, i.e. the ratio of the core window area occupied with copper. This is heavily determined by the selected winding technology and for HV transformers the values range between 0.05 and 0.2 [32]. There are several factors which can decrease this value, particularly when pipes are used as windings. Firstly, compared to rectangular conductors, round conductors do not pack perfectly. In the optimal case of solid round conductor with no insulation, the fill factor takes maximally 0.785 of the unit square. Secondly, the inner channel of the pipe conductor takes the highest portion of the copper area, due to high frequency operation, as discussed earlier. Assuming the wall thickness amounts to 10% of the pipe's OD, which now makes 0.36 of unity of solid round conductor, the fill factor reduces to $0.785 \cdot 0.36 \approx 0.28$. However, with the application that is considered in this paper and the selection of oil insulation, additional space needs to

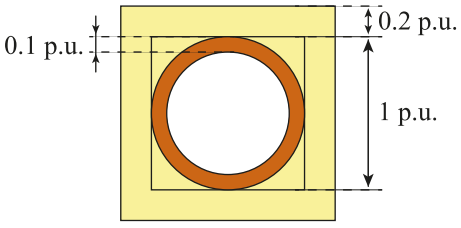

FIGURE 11. Illustration of a copper pipe cross section immersed in insulation liquid to support the fill factor estimation in the core window area. The indicated sizes are given as per unit distances, with a base example distance of 10 mm.

be assigned to the insulation as well. It can be assumed that per turn additional 20% of the unit square needs to be left for the insulation fluid. Eventually, this reduces the fill factor of the new square unit of size 1.4·1.4 to 0.14, which is illustrated in Fig. 11. The obtained fill factor estimation needs to be further reduced when the lost window area is considered, which is marked red in Fig. 12a, due to the required space that the winding needs in order to make a circular turn around the core cross section. A rough estimate is that the lost area amounts to 40% of the considered window area. Finally, this reduces the fill factor to below 0.09. An alternative to increase the utilization factor of the window area is to avoid circular windings and opt for a more complex winding structure, as illustrated in Fig. 12b, which can be applied as well for rectangular core cross sections. In this case, the area lost to necessary distances between the core and vessels can be estimated to 15%, which would increase the fill factor to 0.12.

Regarding the copper cross section and the resulting current density, depending on the nominal MFT operation, the values need to be considered together with the overall thermal coordination and available cooling capabilities. In general, with active cooling present, current densities of 15 A mm^{-2} to 20 A mm^{-2} can be managed.

C. MECHANICAL WITHSTAND CAPABILITIES

In the winding design phase, it is important to consider the mechanical stresses that the transformer can be submitted to during abnormal conditions. Electromagnetic axial and radial forces are generally exerted on the windings in regular operation. However, in the case of in-rush or short-circuit currents in different fault conditions, these forces reach substantial values which can deform or even destroy the windings. The forces increase due to high current values passing through the windings and the magnified leakage field owing to the core saturation. Regarding the effect, the radial components act to reduce the radius of the inner winding and to increase the radius of the outer winding, whereas the axial forces compress the windings to reduce their height.

Therefore, these destructive forces need to be predicted already in the design phase, so that clamping mechanisms can

be designed in order to avoid breakdowns at a later stage. For this purpose, analytical models [33], [34] exist, which are usually verified with time stepping finite element method (FEM) simulations. Another way is to directly use FEM simulations [35], [36]. Both methods require previous estimation of short-circuit and in-rush currents. Additionally, the leakage field can be reduced with interleaving of the windings, which would decrease the magnitude of electromagnetic forces and consequently the mechanical stress applied to the windings [35].

IV. WINDING INDUCTANCE MODELING

For correct operation of the selected converter topology (resonant LLC converter), the windings' intrinsic parameters, such as leakage and magnetizing inductance, have to match the needs of the converter and fall in certain range. The leakage inductance value is determined by the windings' geometry, i.e. by the magnetic energy stored primarily in the interwinding space, whereas the magnetizing inductance is additionally influenced by the core geometry as well. Consequently, accurate and reliable models are necessary to model the relevant inductances. In addition, the influence of relative position of PW to SW on the leakage inductance is studied and the results are presented.

As already mentioned, for the selected converter topology, the two characteristic winding inductances make the bigger part of the resonant tank. More importantly, the magnetizing inductance directly impacts the turn-off current of the semiconductor devices and consequently, the resulting switching losses [25]. Its value can be simply determined with the help of the following equation [27]:

$$L_{\mathrm{m}} = \frac{\mu_0 A_{\mathrm{c,eff}} N_{\mathrm{PW}}^2}{l_{\mathrm{ag}} + \frac{\mathrm{MPT}}{\mu_{\mathrm{r}}}} \tag{5}$$

It is valid in case the fringing flux around the air gap is not considered, which is accurate for sufficiently small air gaps. Thereby, $A_{\mathrm{c,eff}}$ and MPT are the core related parameters describing the effective core cross section area and the magnetic path length, whereas μ_{r} is the relative magnetic permeability of the magnetic material. l_{ag} gives the total air gap length.

The leakage inductance can be estimated in several ways, such as with the help of numerical methods with FEM softwares, which are very accurate but time consuming and heavy on resources; reluctance network models, which are faster but less accurate; and analytical methods, which are fast to compute, reliable and suitable for design optimization tools. A thorough and detailed comparison of analytical and semi-analytical leakage inductance estimation methods is given in [37] and [38].

The leakage inductance model adopted in this paper is of analytical nature and developed by Margueron [39], which utilizes the method of magnetic images from [40]. The idea is to replace the magnetic material with current sources located on the magnetic side, symmetrical to the winding currents in the core window area. Thereby, the current magnitude is set to preserve the initial magnetic field in the air. In this way, the method is able to capture the effect of transformer core on the leakage inductance.

In the model, the total leakage inductance is determined based on the magnetic energy stored in and around the windings, assuming zero magnetizing current. This is achieved in case when the transformer is supplied with two currents of opposite directions whose ratio corresponds to the turns ratio, i.e. the total current in the core window area is zero and the magnetic energy is solely stored in the leakage inductance. The transformer windings are modeled as rectangular winding blocks. Note that the applied model is able to determine only the static values of the inductance, i.e. it is valid for low frequencies where the eddy-current effect is negligible and it can be assumed that the current density is uniform in the conductor.

The implemented method is referred to as Double-2D leakage inductance modeling, since it considers separate estimation of the per unit length leakage inductances in the inside ($L'_{\sigma,IW}$) and the outside core window area ($L'_{\sigma,OW}$), marked with IW and OW, respectively. Based on the corresponding partial lengths of the windings, $l_{\mathrm{w,in}}$ for IW and $l_{\mathrm{w,out}}$ for OW which are shown in Fig. 14, the total leakage inductance is estimated with the following relation

$$L_\sigma = L'_{\sigma,IW} \cdot l_{\mathrm{w,in}} + L'_{\sigma,OW} \cdot l_{\mathrm{w,out}}. \tag{6}$$

Explicit equations, which are derived based on the complete analytical static leakage inductance calculation from [39] for the 2-vessel MFT structure, which implies four windings inside of the core window area, are not presented here due to lack of space. Note that the selected analytical model considers all the winding types as rectangular blocks. With the help of FEM simulations, it can be observed whether this provides an accurate estimation for pipe windings.

A. SENSITIVITY ANALYSIS

Having in mind that for valid operation of the resonant LLC converter, the leakage inductance needs to be closely targeted, a study was conducted in order to examine the sensitivity of

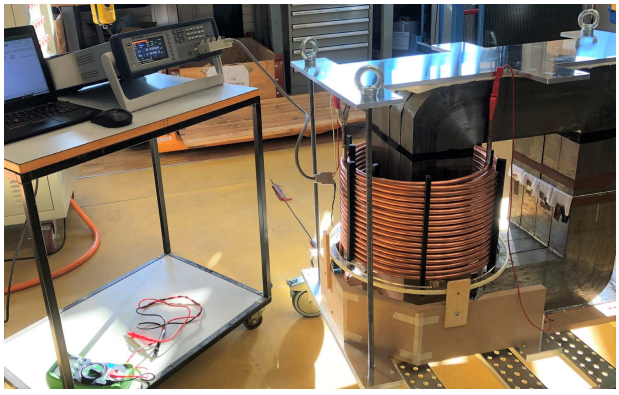

FIGURE 13. Setup used to study the sensitivity of the leakage inductance depending on the relative position of PW to SW.

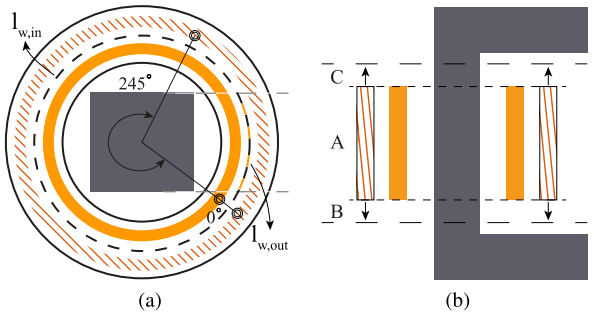

FIGURE 14. (a) Top cross sectional view of the one half of the considered 2-vessel MFT structure. Winding terminations are illustrated with round pipe cross sections. $l_{w,in}$ and $l_{w,out}$ mark the portions of the mean length turn inside and outside of the core window area, respectively. (b) Front view of an MFT half. A, B and C mark the relative positions of PW to SW, corresponding to 0 cm, −1 cm and +1 cm, respectively.

this intrinsic value to the position of PW and SW terminations relative to each other. Additionally, the effect of vertical disposition between the windings is observed.

Fig. 13 shows the setup to measure the sensitivity of leakage inductance at the PW side in response to slight changes in the relative position of PW to SW. For this purpose, a single winding set is observed, made of one layer of PW and one layer of SW with the same number of turns and wound with the same copper pipe. To observe the influence, the position of SW is fixed, whereas the PW is able to rotate around the SW in steps of 5°, reaching from 0° to 245°. Accordingly, the PW is fixed to a plexiglass ring, which is able to rotate around one of the core limbs. The ring is calibrated with 5° markings and functions as a protractor. Thereby, parallel terminations of both windings correspond to the angle of 0°, whereas the upper limit angle corresponds to the terminations being at the opposite sides of the core, as illustrated in Fig. 14a.

To perform the measurements two different measuring devices are used, namely, an RLC meter (BK895), which measures impedances at fixed frequencies (marked as measuring method M_1) and an impedance analyzer Bode 100 by Omicron Lab (marked as M_2). The measuring frequency for both devices is set to 5 kHz. Fig. 15 shows the measuring results for three selected cases: A) PW and SW are at the same height; B) PW is set 1 cm lower than SW and C) 1 cm higher than SW. Note that the values in the graphs do not correspond to the total leakage inductance of the final MFT prototype, since only a single set of PW and SW is observed.

First observation from Fig. 15 is that the measurements performed with two different devices give matching results. Regarding the leakage inductance sensitivity to a change in angle, i.e. position between the PW and SW terminations, which contributes to slight vertical deviation in windings' heights, no significant dependency can be observed. Yet, slight ripples in the inductance value (below 1 µH) are detected as the angle increases, which can be ascribed to measurement errors. Lastly, results of case B and C exhibit very similar values, which is to be expected since the windings' surfaces overlap in the same extent, regardless whether PW is lifted higher or lower for the same amount of distance.

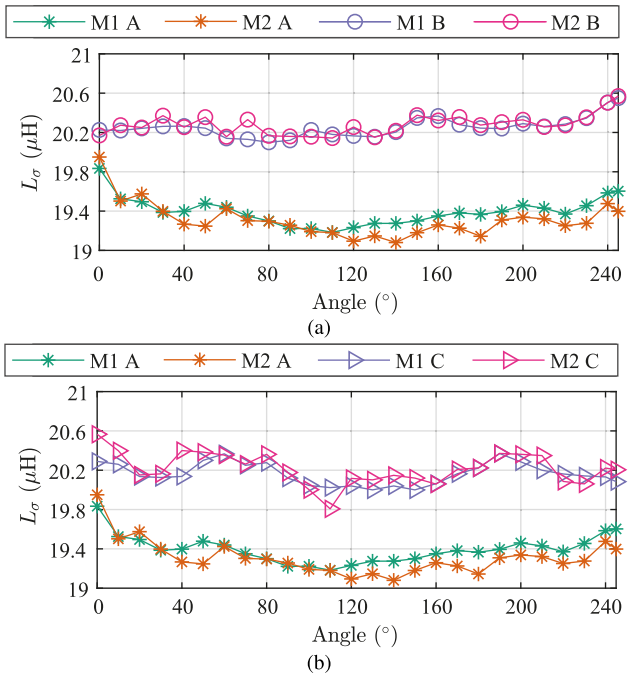

FIGURE 15. Influence of PW to SW relative position on the leakage inductance in case when (a) PW is set 1 cm lower (case B) and (b) 1 cm higher than SW (case C). The orange and green show measurements when the PW and SW are at the same height, which corresponds to case A from Fig. 14b. They are repeated in both graphs for comparison purposes.

V. ELECTRICAL RESISTANCE MODELING

To appropriately size and design a cooling system for the considered DCT, it is necessary to have accurate estimation of the converter losses, and more particularly in the case of the MFT, correctly estimate the winding losses. Depending on the winding geometry, the type of conductor used, the surrounding currents and the operating frequency, transformer windings can experience skin and proximity effects. This in turn makes the winding loss estimation more challenging. An overview and a comparison of the existing models, which address the most common winding geometries, is presented in [41]. So far, the basis of many analytical models used nowadays is the Dowell's model [42], developed for foil windings under a certain set of assumptions and based on the solution of electromagnetic equations in 2D. As a result, the model provides a frequency dependent expression for AC resistance of the winding by introducing a resistance factor F_r, as a multiplier of the DC resistance. Thus, it can be used to calculate losses for various current harmonics. Moreover, the model can be adjusted to other winding geometries with the help of the porosity factor η. Its purpose is to ensure that an equal magnetic field is generated along an enclosed path for two different winding types. Since the geometry change effects the copper cross section area, the porosity factor needs to adjust the effective conductivity of the surface. Correspondingly, the winding porosity factor represents the ratio of the actual layer copper area to the foil conductor area extending the full core window height, and it is visualized in Fig. 16. The porosity factor can be expressed as a multiplication of the factors $\eta_1 - \eta_3$ which show the

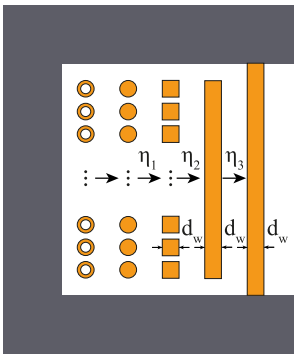

FIGURE 16. Illustration of applying the Dowell's model, from pipes to foil windings which extend over the full window height of the size H_w.

adjustment of the winding geometry in several steps. Based on the Dowell's model, the AC resistance is defined by

$$R_{ac} = F_r R_{dc} = \Delta \underbrace{\frac{\sinh(2\Delta) + \sin(2\Delta)}{\cosh(2\Delta) - \cos(2\Delta)}}_{\text{skin effect factor}} R_{dc} + \frac{2}{3}(m^2 - 1)\Delta \underbrace{\frac{\sinh(\Delta) - \sin(\Delta)}{\cosh(\Delta) + \cos(\Delta)}}_{\text{proximity effect factor}} R_{dc}, \quad (7)$$

with the parameter $\Delta = \frac{d_w}{\delta_{Cu}}\sqrt{\eta}$, known as the penetration ratio. The parameters d_w and m stand for the thickness of the foil conductor and the number of winding layers. Thereby, skin and proximity correction factors are clearly marked in the equation above. They can be neglected for low frequencies, i.e. where the penetration factor is smaller than 1, but their values increase significantly for $\Delta > 1$, i.e. for higher frequencies [41]. It is generally assumed that eddy current densities caused by these two effects inside a specific winding layer are orthogonal, which allows for an easier calculation of winding losses.

However, pipe windings present a unique type of conductors, particularly due to their geometry, which is not sufficiently researched in the literature. To estimate the pipe winding losses an additional resistance factor is adopted from [43], termed as the hollow resistance factor F_h. It is obtained with the help of FEM simulations and determined particularly for hollow conductors, defined by the following equation

$$F_h = \frac{R_{ac,h}}{R_{ac,s}}, \quad \text{with } R_{ac,s} \text{ defined in (9).} \quad (8)$$

Accordingly, the Δ parameter is redefined as the hollow penetration ratio $\Delta_h = \frac{\delta}{\delta_{Cu}}$. Note that the first step from the hollow to the solid round conductor, shown in Fig. 16, is traversed with the hollow resistance factor. The value is determined with the help of numerous 2D simulations, looking into models with $1 - 3$ winding layers, several ODs of the conductor (8 mm, 9 mm and 10 mm) and a wide range of Δ_h from $(0.6 - 2.5)$, i.e. various wall thicknesses, and a range of operating frequencies [2 kHz - 10 kHz]. Detailed explanations regarding the extracted resistance factor and the conducted FEM simulations can be found in [43].

Eventually, the total power loss experienced by a winding conducting the current I is given by

$$P_{loss} = \underbrace{\frac{MLT}{\eta\sigma d_w H_w}}_{R_{dc}} I_{dc}^2 + \sum_{n=1}^{\infty} R_{ac,n} I_{rms,n}^2, \quad (9)$$

where n stands for the harmonic order of the winding current, σ is the copper conductivity and MLT is the corresponding mean length turn of the foil winding.

VI. THERMAL MODELING

There are many ways transformer winding insulation can be achieved depending on the blocking voltage and the target power density. The main insulation concepts rely on air, solid or oil as insulating media. Compared to the other two options, air as insulator features the weakest dielectric properties, providing a breakdown voltage of ≈ 3 kV. Moreover, depending on the percentage of humidity and polluting particles in the air the value reduces to 1 kV. Nevertheless, the use of air allows for combined insulation and cooling, with the help of natural or forced convection. Secondly, cast resin windings improve the power density compared to air, due to increase of breakdown voltage to around 45 kV [44]. This has a positive effect on decrease of necessary insulation distances. However, without a proper cooling implementation, the use of solid insulation can impair the cooling aspect due to low thermal conductivity of cast resin material. Lastly, oil insulation exhibits slightly superior dielectric properties with values of 47 kV of breakdown voltage at 1 mm gap [45]. Similar to air, it offers combined cooling capabilities with the same heat exchange mechanisms. One can conclude that thermal and insulation coordination must be considered together since they impact each other significantly.

Fig. 17 illustrates the 2D cross-sectional axisymmetric front view of a single oil vessel from Fig. 3, which contains a pair of PW and SW, simplified as foil windings. Note that

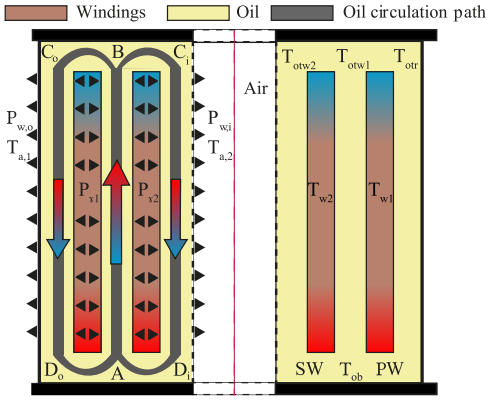

FIGURE 17. 2D front view of an axisymmetric single oil vessel containing windings simplified as foil conductors. Blue and red colors indicate respectively lower or higher temperatures of copper or oil.

the inner space of the vessel is occupied by air and not by a core limb, which is the case for a functional MFT. Therefore, the model considers two different ambient temperatures, $T_{a,1}$ and $T_{a,2}$, corresponding to the exterior air temperature and inside of the inner tube of the vessel, respectively. The axis of symmetry is marked with the red dashed line in the middle. The windings assume average temperatures of T_{w1} and T_{w2}, which are determined based on the copper temperatures measured or estimated at the top and bottom of the conductors outside of the oil vessel. In the steady state PW and SW release in the surrounding oil the losses $P_{\gamma 1}$ and $P_{\gamma 2}$, respectively, which represent a small portion of the total winding losses. The exact values are obtained by estimating the percentage of losses that did not get absorbed by the DI water passing through the windings. The estimation is based on the temperature difference of the coolant entering and exiting the windings and the information about the dissipated winding losses. By knowing the WCU operating point, i.e. the volumetric flow and the inlet and outlet water temperature, it is possible to determine the amount of absorbed losses with the following equation

$$P_{\mathrm{DI,w}} = \dot{m} c_{\mathrm{p}} \Delta T_{\mathrm{w}}. \tag{10}$$

The parameter $\dot{m}$ describes the volumetric flow of the coolant, c_{p} is its specific heat capacity and ΔT_{w} gives the water temperature increase from the outlet to the inlet due to winding loss absorption. Eventually, the excess winding losses that heat the oil are obtained by subtracting the absorbed from the total winding losses.

As previously mentioned in Section II, a consequence of the initial choice to assign the DI water inlet to the windings' top is a temperature gradient, which is formed along the windings in the vertical direction. The gradient starts at the top with a lower temperature and increases to a higher temperature at the bottom of the windings. This is visualized with blue and red color of foil windings in Fig. 17, respectively. Increased temperature at the bottom causes the surrounding oil to warm up, leading to a decrease in mass density and oil expansion. In this way buoyancy forces form which drive the oil upwards, i.e. from points A to B. This is indicated with a vertical colored arrow, illustrating the oil temperature change from blue/cold to red/hot. At the top, the oil starts to cool down experiencing an increase in mass density, due to better cooling of the windings. The fluid becomes heavier and descends back to the bottom, cooling as it moves along the paths C_o to D_o and C_i to D_i, marked with downward vertical arrows. Additional heat exchange takes place between the oil and the vessel walls, marked with $P_{\mathrm{w,o}}$ and $P_{\mathrm{w,i}}$, for the outer and the inner wall, respectively. In steady state two oil paths are formed, namely, ABC_oD_oA and ABC_iD_iA. In this way natural oil convection and circulation are achieved, which confirms the self-healing properties of the insulation liquid. In practice, due to oil expansion, a supplementary vessel needs to be added to the vessel with windings. Another solutions is to leave an air pocket of sufficient size inside of the vessel, to allow the oil to spread when heated.

Considering specific combination of technologies, i.e. forced water cooling and natural-convection based insulation, the authors developed a thermal-hydraulic model (THM) [46]. The THM describes the thermal behavior of the insulation oil and it is able to accurately estimate characteristic oil temperatures (T_{ob}, T_{otw1}, T_{otw2} and T_{otr}), depending on the winding losses and the cooling conditions. The model implementation is based on analytical equations, describing the thermal and the hydraulic sides of oil circulation caused by natural convection, combined with thermal measurements and multi-objective optimization. The solution requires consideration of the hydraulic side of the problem as well, since moving oil causes pressure drops. Full description of the developed model including the analytics can be found in [46].

The experimental measurements are collected with the help of a down-scaled test setup shown in Fig. 18a. It is comprised of a single oil vessel with a set of PW and SW (15 turns for each winding, wound with a copper pipe of an inner diameter of 5.2 mm and a wall thickness of 1.4 mm) with a fixed inter-winding distance and immersed in synthetic ester dielectric oil (Midel 7131). To measure characteristic oil temperatures, 18 thermocouples (TCs) are added equidistantly in the same vertical plane which passes through the vessel center. Five TCs, marked with $T_1 - T_5$, are placed at the vessel top and five at the bottom, marked with $B_1 - B_5$. The rest of TCs ($S_1 - S_8$) are inserted on the side, exactly between the outer vessel wall and the PW, as illustrated in Fig. 18b. Moreover, additional four TCs are attached to the top and bottom parts of the copper pipes outside of the vessel, to have a notion about the copper temperature. To emulate conduction losses, the PW and SW are connected in series and to a controlled DC power supply. For cooling purposes, transparent hoses are attached to each winding side, distributing and collecting DI water from and to a WCU of controlled temperature and volumetric flow.

In the next step, with the help of multi-objective optimization, more specifically, with the genetic algorithm, the difference between experimentally obtained and analytically modeled characteristic oil temperatures is minimized. At the same time, the pressure balance in the two oil loops is

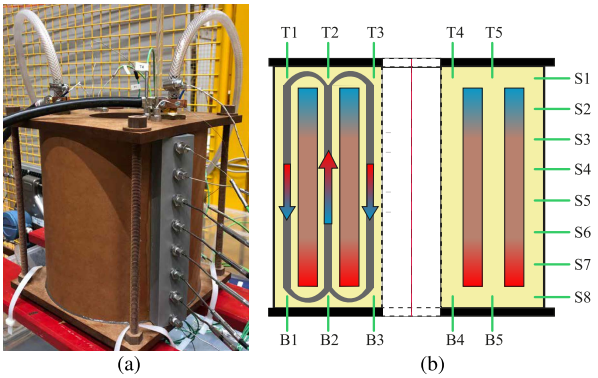

FIGURE 18. (a) Vessel with oil and a pair of PW and SW connected to a DC power source and DI WCU. Thermal measurements of oil are collected with 18 thermocouples, placed inside of the vessel according to (b).

TABLE 3. Winding-specific characteristics of an optimal 2-vessel MFT design, selected based on the highest efficiency criterion (99.18%). The pressure drop along the PW and SW corresponds to a volumetric flow of 1.8 cls^{-1}.

$D_{\mathrm{i,PW,SW}}$	$\delta_{\mathrm{PW,SW}}$	N_{PW}	N_{SW}	$R_{\mathrm{a,PW}}$	$R_{\mathrm{a,SW}}$	$J_{\mathrm{PW,SW}}$
7.6 mm	1.3 mm	34	17	17.5 cm	15.5 cm	6.1 A mm^{-2}
$P_{\mathrm{loss,PW}}$	$P_{\mathrm{loss,SW}}$	Δp_{PW}	Δp_{SW}	l_{PW}	l_{SW}	R_{wc}
2.87 kW	2.67 kW	5.18 kPa	4.64 kPa	37.8 m	33.9 m	0.32

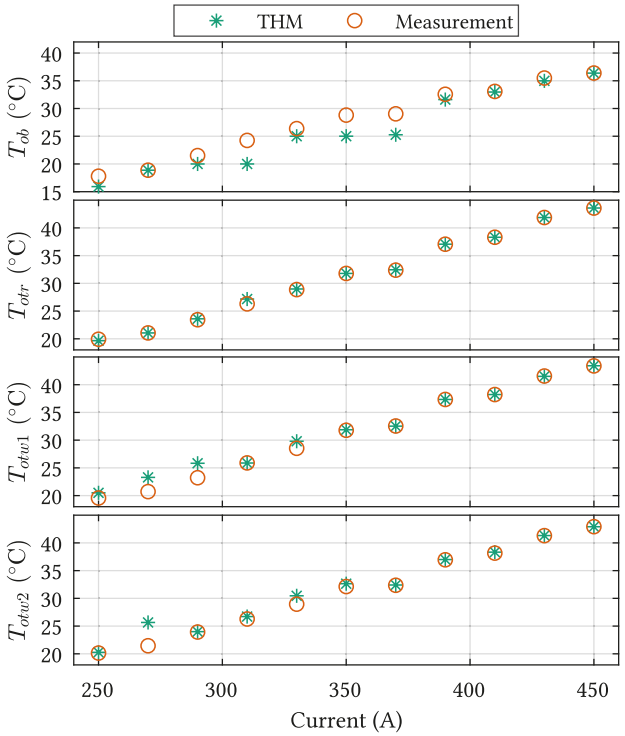

FIGURE 19. Comparison of experimentally obtained oil temperature measurements with the analytical THM results for various operating points (DC current supply of f 250 A - 450 A corresponds to total winding losses of approximately 1 kW - 3 kW).

maintained. Finally, Fig. 19 compares characteristic oil temperatures estimated by the THM with the gathered thermal measurements for several operating points. An overall good agreement between the two can be observed. Notably, the accuracy of the analytical model tends to improve with higher injected currents, since the deviation between measured and modeled, for all four observed oil temperatures, and for the same operating point remains very small.

VII. 1 MW, 5 kHz MFT PROTOTYPE

After all the models, challenges and remarks have been answered and covered, a design of copper pipe windings intended for a 1 MW MFT prototype is realized. The properties of the transformer windings design are given in Table 3. It provides information about the characteristic pipe winding properties, regarding the geometry, nominal conduction losses and pressure drops, that were discussed and modeled in

TABLE 4. Comparison of the analytical leakage inductance values with FEM simulations for 2-vessel MFT structure, which model the windings as foil and pipe. All the values are frequency-independent.

	An. model	FEM 2D foil	FEM 2D pipe
$L'_{\sigma,\mathrm{IW}}$ (µH m^{-1})	43.12	42.56	44.53
$L'_{\sigma,\mathrm{OW}}$ (µH m^{-1})	41.15	40.97	42.81
$L_{\sigma,\mathrm{tot}}$ (µH)	43.8	43.71	45.94

previous sections. In addition, the information about the core to winding loss ratio (R_{wc}) is provided. The values for loss, pressure and length include summed values of both winding parts from the two vessels. Note that the presented winding design does not include mechanical withstand capability considerations.

For implementation of transformer windings as described in Table 3, pipes made of soft temper copper are used and are produced by Luvata [9]. Per design, the wall thickness of the pipe is selected higher than the skin depth at the frequency of 5 kHz and corresponds to a hollow penetration ratio of $\Delta_h \approx 1.4$. Such decision can be traced back to the hollow resistance factor, which is for this frequency and wall thickness slightly lower than 1. Therefore, the theoretical conduction losses from Table 3 need to be verified experimentally. The nominal current density of the selected design is well below the stated capabilities of pipe windings from Section III-B and this is due to the fact that the design focus is set on achieving the highest efficiency.

Note that the right temper selection significantly aids the manipulation. Regardless, winding of copper pipes to obtain two PW and SW sets of 17 turns each, with specified external winding radii and a fixed turn-to-turn distance (v_{d}), proved to be a challenging task. Following the discussion regarding the necessary v_{d} from Section III-A, the value is set to 3 mm. Fig. 20a shows the method that is used for winding of the copper pipes into the necessary form, for the task of transformer windings. The method belongs to the mandrel bending approach, shortly introduced in Section III-A. A description of the procedure is summarized in the following. A wooden mandrel of appropriate cross section diameter is attached to a rotating shaft with an additional structure (framed in white) mounted in its vicinity to guide the copper pipe onto the mandrel. Additionally, a similar fixing structure (framed in black) is added directly on the mandrel to keep the pipe in

(a) (b) (c)

FIGURE 20. (a) Method used to make transformer windings of the correct external radius using copper pipes; MFT oil vessels, made of phenolic paper composite material Etronit I and B66, each containing a set of PW and SW with spacers and the insulation liquid: (b) Left vessel; (c) In between the vessels.

place during the rotation. Nevertheless, due to high mechanical strength of even soft temper copper, at the moment the winding is released from the mandrel it loosens and increases its initially intended external radius. This practical challenge is resolved by trial and error method, i.e. by readjusting the outer diameter of the mandrel until the correct external winding radius is achieved.

Fig. 20b and 20c show the two oil vessels made of phenolic paper composite material, manufactured by Elektro-Isola [47], with windings and insulation fluid inside. As can be noticed, an air pocket of sufficient size is left at the top of each vessel, which allows the fluid to expand from an ambient temperature to 80 °C. For the excess of air during the expansion, two additional outlets are added at the top of each vessel, which are connected to two air breathers filled with silica gel. Their task is to act as purifying and drying agents, thus keeping the moisture and particles away from the oil. In addition, to improve stability and ensure correct distances and positioning inside of each vessel, comb-alike spacers introduced in Section III-A are added to each winding. Note that for this prototype, the spacers are not intended to be used as winding clamping mechanism, which is designed to prevent damage in the case of excessive electromagnetic forces under fault conditions. For the considered MFT prototype, both PWs are wound the counterclockwise direction looking from the top, whereas the SWs are wound reversely. The full prototype assembly is discussed in details in [48].

The validity of the used leakage inductance model, presented in Section IV, for the considered winding arrangement has been confirmed with 2D FEM simulations. Two different winding types are modeled and simulated in COMSOL. The results are shown in Table 4. Thereby, FEM 2D foil simulation models the windings as foils, which are also assumed for the analytical model, whereas FEM 2D pipe uses perfect helices. Eventually, a very good matching between the analytics and FEM 2D foil simulations is not surprising. It can be further observed that the analytical model slightly underestimates the leakage inductance obtained with pipe windings FEM simulations. Note that both 2D models are achieved as vertical cross sections of the corresponding 3D models. However, the results from Table 4 address the static leakage inductance estimation. In reality, the eddy current effect present at elevated frequencies reduces the DC value. Its influence can be observed either with FEM simulations or directly with the help of measurements, as shown in Table 5. Concerning 2D FEM simulations, frequency-dependent studies were conducted, which solve the standard set of Maxwell's equations, with automatic physics-controlled triangular meshing with finer element size, and default direct solver setting.

As shortly discussed in Section IV, the magnetizing inductance dictates the MFT magnetizing current, i.e. the turn-off current for the selected converter topology. The reference value from Table 5 corresponds to the total air gap of 1 mm, which is equally distributed between two core limbs, and it implies a turn-off current of 7 A. Both leakage and

TABLE 5. Comparison of measured and modeled MFT leakage and magnetizing inductances.

L_σ (µH)	An. model	FEM 2D pipe	RLC	Bode 100
at 5 kHz	–	34	38.2	37.9

L_m (mH)	Ref. value	RLC	Bode 100
at 5 kHz	35.77	36.66	36.74

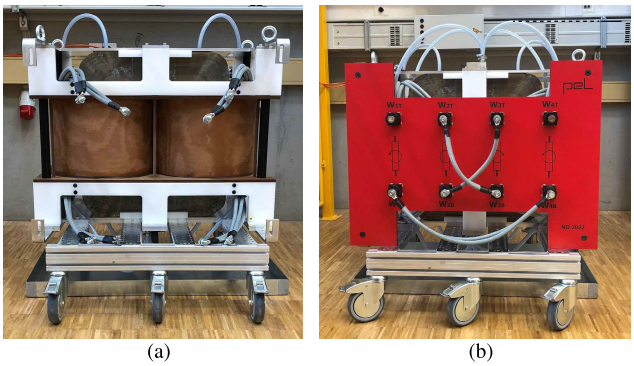

(a) (b)

FIGURE 21. 1 MW prototype of the 2-vessel MFT (a) without and (b) with the winding termination panel and the top and bottom DI water distribution units.

magnetizing inductances are measured at the primary side and they match the simulated and the modeled values.

Finally, Fig. 21 shows the 1 MW MFT prototype. Fig. 21a presents the MFT without the DI water distributors at the top and bottom, and the winding termination panel, which are included in Fig. 21b. The addition of panel further simplifies connection of the prototype to the power stages and forming of the necessary turns ratio.

VIII. CONCLUSION

This paper presents an overview of all the aspects which need to be considered when using round copper pipes as MFT windings. The conducted study shows that it is feasible to use them in this way, and it has already been done in recorded literature, however, aluminum was used as winding material. The inner channel of the pipe is utilized for forced DI water cooling, though other types of liquid coolants can be used as well. Nevertheless, the complete design needs to include a cooling unit. Direct benefits when using this technology are increased power and current density. Additionally, several technical difficulties are discussed, such as mechanical constraints and issues regarding practical realization.

Conclusions in the form of design guidelines for copper pipe windings are summarized in the following:

- From available pipe manufacturers' information, MFT designs up to 10 kHz can be realized with copper pipes having wall thicknesses up to 0.6 mm.
- To facilitate the winding process, it is recommended to choose soft temper copper and mandrel bending approach.
- To keep stability and fixed distances between two turns and the windings in general, supporting structures need to be added.
- If the core cross section requires large area, which implies that a sizeable part of the core window area remains unused due to the necessary winding curvature, the pipes can be wound semi-circular with straight portions. In this way, these parts can be placed closer to the core inside of the window area, which helps to improve the total fill factor. Nevertheless, this additionally complicates the winding process.
- The relative position of winding terminations to each other do not effect the resulting leakage inductance. Yet, sufficient space should be left between to ensure proper isolation.
- Thermal coordination of pipe windings has to be combined with cooling capabilities and insulation coordination for an optimal MFT design in general.

Lastly, the presented 1 MW MFT measures the weight of 462 kg, which translates to 2.17 kW kg^{-1} of gravimetric and 1.59 kW l^{-1} of volumetric power density. According to the selected design the optimal current density in all the windings is slightly above 6 A mm^{-2}. At the nominal operating point, the total winding losses are estimated to roughly 5.5 kW.

REFERENCES

[1] J. E. Huber and J. W. Kolar, "Solid-state transformers: On the origins and evolution of key concepts," *IEEE Ind. Electron. Mag.*, vol. 10, no. 3, pp. 19–28, Sep. 2016.
[2] G. Ortiz, "High-power DC–DC converter technologies for smart grid and traction applications," Ph.D. dissertation, Power Electron. Syst. Lab., ETH Zürich, Zürich, Switzerland, 2014.
[3] S. Kim, G. Ulissi, S.-N. Kim, and D. Dujic, "Marine DC power distribution networks," in *Proc. PCIM Europe Int. Exhib. Conf. Power Electron., Intell. Motion, Renew. Energy Energy Manag.*, 2019, pp. 1–8.
[4] U. Javaid, D. Dujic, and W. van der Merwe, "MVDC marine electrical distribution: Are we ready?" in *Proc. IECON 41st Annu. Conf. IEEE Ind. Electron. Soc.*, Nov. 2015, pp. 823–828.
[5] C. R. Sullivan, "Optimal choice for number of strands in a Litz-wire transformer winding," *IEEE Trans. Power Electron.*, vol. 14, no. 2, pp. 283–291, Mar. 1999.
[6] E. Ramchy, B. Malinowska, and M. Cassir, "Design of de-ionised water cooling of power converters," in *Proc. 29th Annu. IEEE Power Electron. Spec. Conf.*, vol. 2, May 1998, pp. 1931–1936.
[7] A. da Silva Dias, D. B. Candido, A. P. Almeida, and J. A. Alves, "Cooling methods design for power electronics converters," in *Proc. Brazilian Power Electron. Conf. (COBEP)*, Nov. 2017, pp. 1–6.
[8] *Deepak Steel India*, India. Accessed: Sep. 26, 2022. [Online]. Available: https://www.deepaksteelindia.com/copper-pipes-tubes-exporter-suppliers
[9] *Luvata Pori Oy, Finland*. Accessed: Sep. 26, 2022. [Online]. Available: https://www.luvata.com/
[10] *Copper Tube & Fittings*. Canadian Copper & Brass Development Corp., Toronto, ONT, Canada 2000.
[11] J. R. Davis, *Copper and Copper Alloys*. OH, USA: ASM International, 2001.
[12] S. Ayat, B. Daguse, and R. Khazaka, "Design considerations of windings formed with hollow conductors cooled with phase change material," in *Proc. IEEE Energy Convers. Congr. Exposit. (ECCE)*, Sep. 2019, pp. 5652–5658.
[13] S. Ayat, C. Serghine, T. Klonowski, S. Yon, A. Mutabazi, and S. McDaniel, "The use of phase change material for the cooling of electric machine windings formed with hollow conductors," in *Proc. IEEE Int. Electric Mach. Drives Conf. (IEMDC)*, May 2019, pp. 1195–1201.
[14] P. Lindh, I. Petrov, A. Jaatinen-Värri, A. Grönman, M. Martinez-Iturralde, M. Satrústegui, and J. Pyrhönen, "Direct liquid cooling method verified with an axial-flux permanent-magnet traction machine prototype," *IEEE Trans. Ind. Electron.*, vol. 64, no. 8, pp. 6086–6095, Aug. 2017.
[15] G. Ridley, "The U.K.'s first direct-water-cooled pumped-storage generator-motor," *Electron. Power*, vol. 28, no. 10, pp. 678–681, 1982.
[16] R. F. Gray, L. Montgomery, R. Nelson, J. Pipkin, S. Joki-Korpel, and F. Caguiat, "Designing the cooling systems for the world's most powerful turbogenerator—Olkiluoto unit 3," in *Proc. IEEE Power Eng. Soc. Gen. Meeting*, Jun. 2006, pp. 1–5.
[17] L. Ruan, F. Liu, and J. Chen, "The selection of hollow conductors for huge evaporative cooling hydrogenerators," in *Proc. Int. Conf. Electr. Mach. Syst. (ICEMS)*, Oct. 2013, pp. 470–473.
[18] R. Lin, G. Guobiao, and T. Xindong, "Research of the temperature distribution of the hollow conductor in the evaporative cooling hydrogenerators," *Electric Power Compon. Syst.*, vol. 33, no. 2, pp. 145–158, Jan. 2005.
[19] H. Hoffmann and B. Piepenbreier, "Medium frequency transformer for rail application using new materials," in *Proc. 1st Int. Electric Drives Prod. Conf.*, Sep. 2011, pp. 192–197.
[20] M. Steiner and H. Reinold, "Medium frequency topology in railway applications," in *Proc. Eur. Conf. Power Electron. Appl.*, 2007, pp. 1–10.
[21] L. Heinemann, "An actively cooled high power, high frequency transformer with high insulation capability," in *Proc. 17th Annu. IEEE Appl. Power Electron. Conf. Exposit. (APEC)*, vol. 1, Mar. 2002, pp. 352–357.
[22] K. W. Klontz, D. M. Divan, and D. W. Novotny, "An actively cooled 120 kW coaxial winding transformer for fast charging electric vehicles," *IEEE Trans. Ind. Appl.*, vol. 31, no. 6, pp. 1257–1263, Nov. 1995.
[23] D. Stamenkovic, U. R. Vemulapati, T. Stiasny, M. Rahimo, and D. Dujic, "IGCT low-current switching—TCAD and experimental characterization," *IEEE Trans. Ind. Electron.*, vol. 67, no. 8, pp. 6302–6311, Aug. 2020.
[24] G. Ulissi, J. Kucka, U. R. Vemulapati, T. Stiasny, and D. Dujic, "Resonant IGCT soft-switching: Zero-voltage switching or zero-current switching?" *IEEE Trans. Power Electron.*, vol. 37, no. 9, pp. 10775–10783, Sep. 2022.
[25] G. Ulissi, U. R. Vemulapati, T. Stiasny, and D. Dujic, "High-frequency operation of series-connected IGCTs for resonant converters," *IEEE Trans. Power Electron.*, vol. 37, no. 5, pp. 5664–5674, May 2022.

[26] L. Collini, *Copper Alloys: Early Applications and Current Performance-Enhancing Processes*. London, U.K.: IntechOpen, 2012.
[27] M. N. Undeland, W. P. Robbins, and N. Mohan, *Power Electronics, Converters, Applications, and Design*. Hoboken, NJ, USA: Wiley, 1995.
[28] *Copper Tube Handbook*. Copper Development Association, New York, NY, USA, 2020.
[29] *Tube Bending Design Guide*, Lister Tube, Redditch, U.K., 2021.
[30] G. O. Brown, "The history of the Darcy-Weisbach equation for pipe flow resistance," *Environ. Water Resour. Hist.*, vol. 38, no. 7, pp. 34–43, 2002.
[31] F. P. Incropera, A. S. Lavine, T. L. Bergman, and D. P. DeWitt, *Fundamentals of Heat and Mass Transfer*. Hoboken, NJ, USA: Wiley, 2007.
[32] R. W. Erickson and D. Maksimovic, *Fundamentals of Power Electronics*. Berlin, Germany: Springer, 2007.
[33] B. M. Ebrahimi, A. Fereidunian, S. Saffari, and J. Faiz, "Analytical estimation of short circuit axial and radial forces on power transformers windings," *IET Gener., Transmiss. Distribution*, vol. 8, no. 2, pp. 250–260, Feb. 2014.
[34] G. P. Peter, "Calculations for short circuit withstand capability of a distribution transformer," *Ann. Fac. Eng. Hunedoara*, vol. 9, no. 3, p. 243, 2011.
[35] P. Huang, C. Mao, and D. Wang, "Analysis of electromagnetic force for medium frequency transformer with interleaved windings," *IET Gener., Transmiss. Distribution*, vol. 11, no. 8, pp. 2023–2030, Jun. 2017.
[36] J. Y. Lee, H. M. Ahn, and J. K. Kim, "Finite-element analysis of short-circuit electromagnetic force in power transformer," *IEEE Trans. Ind. Appl.*, vol. 47, no. 3, pp. 1267–1272, May/Jun. 2011.
[37] R. Schlesinger and J. Biela, "Comparison of analytical models of transformer leakage inductance: Accuracy versus computational effort," *IEEE Trans. Power Electron.*, vol. 36, no. 1, pp. 146–156, Jan. 2021.
[38] A. Fouineau, M.-A. Raulet, B. Lefebvre, N. Burais, and F. Sixdenier, "Semi-analytical methods for calculation of leakage inductance and frequency-dependent resistance of windings in transformers," *IEEE Trans. Magn.*, vol. 54, no. 10, pp. 1–10, Oct. 2018.
[39] X. Margueron, A. Besri, P.-O. Jeannin, J.-P. Keradec, and G. Parent, "Complete analytical calculation of static leakage parameters: A step toward HF transformer optimization," *IEEE Trans. Ind. Appl.*, vol. 46, no. 3, pp. 1055–1063, May/Jun. 2010.
[40] P. Hammond, "Electric and magnetic images," *Proc. IEE*, vol. 107, no. 12, p. 306, 1960.
[41] I. Villar, "Multiphysical characterization of medium-frequency power electronic transformers," Ph.D. dissertation, Laboratoire d'Électronique Industrielle, EPFL, Lausanne, Switzerland, 2010.
[42] P. Dowell, "Effects of eddy currents in transformer windings," *Proc. Inst. Electr. Eng.*, vol. 113, no. 8, p. 1387, 1966.
[43] F. Lü, Y. Guo, Y. Wang, D. Yu, and P. Li, "AC resistance calculation method for hollow conductor windings in high power medium frequency transformers," in *Proc. CSEE*, vol. 23, 2016, pp. 6552–6558.
[44] T. B. Gradinger, U. Drofenik, and S. Alvarez, "Novel insulation concept for an MV dry-cast medium-frequency transformer," in *Proc. 19th Eur. Conf. Power Electron. Appl. (EPE ECCE Europe)*, Sep. 2017, p. 10.
[45] *Midel 7131 Selection Guide*. Accessed: Sep. 26, 2022. [Online]. Available: https://www.midel.com/app/uploads/2018/05/MIDEL-Selection-Guide.pdf
[46] N. Djekanovic and D. Dujic, "Modeling and characterization of natural-convection oil-based insulation for medium frequency transformers," in *Proc. IEEE Appl. Power Electron. Conf. Exposit. (APEC)*, Mar. 2022, pp. 604–610.
[47] *Elektro-Isola A/S*. Accessed: Sep. 26, 2022. [Online]. Available: https://www.elektro-isola.com/
[48] N. Djekanovic and D. Dujic, "Design optimization of a MW-level medium frequency transformer," in *Proc. PCIM Europe Int. Exhib. Conf. Power Electron., Intell. Motion, Renew. Energy Energy Manag.*, 2022, pp. 1–10.

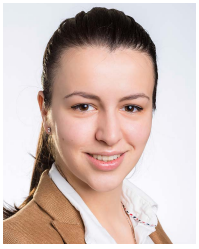

NIKOLINA DJEKANOVIC (Graduate Student Member, IEEE) received the B.Sc. and Dipl.-Ing. degrees from the Vienna University of Technology (TU Wien), Vienna, Austria, in 2016 and 2018, respectively. She is currently pursuing the Ph.D. degree with the École Polytechnique Fédérale de Lausanne (EPFL), Lausanne, Switzerland.

During the M.Sc. degree, she spent one year at the KTH Royal Institute of Technology, Stockholm, Sweden, as an Exchange Student and a Research Engineer. In 2019, she joined the Power Electronics Laboratory, EPFL, as a Doctoral Research Assistant. Her research interests include modeling, design, and optimization of high-power medium-voltage transformers, power electronics, and batteries.

DRAZEN DUJIC (Senior Member, IEEE) received the Dipl.-Ing. and M.Sc. degrees in electrical engineering from the University of Novi Sad, Novi Sad, Serbia, in 2002 and 2005, respectively, and the Ph.D. degree in electrical engineering from Liverpool John Moores University, Liverpool, U.K., in 2008.

From 2002 to 2006, he was a Research Assistant with the Department of Electrical Engineering, University of Novi Sad. From 2006 to 2009, he was a Research Associate with Liverpool John Moores University. From 2009 to 2013, he was with ABB Corporate Research Center, Switzerland, as a Principal Scientist, working on the power electronics projects spanning the range from low-voltage/power SMPS in below kilowatt range to medium voltage high-power converters in a megawatt range. From 2010 to 2011, he was a member of a project team responsible for the development of the world's first power electronic traction transformer successfully commissioned on the locomotive. From 2013 to 2014, he was with ABB Medium Voltage Drives, Turgi, Switzerland, as a Research and Development Platform Manager, responsible for ABB's largest IGCT-based medium voltage drive ACS6000. He is currently with the École Polytechnique Fédérale de Lausanne (EPFL), Lausanne, Switzerland, as an Associate Professor and the Director of the Power Electronics Laboratory. He has authored or coauthored more than 200 scientific publications and has led 18 patents. His current research interest includes design and control of advanced high-power electronics systems for medium voltage applications.

Dr. Dujic has received the First Prize Paper Award from the Electric Machines Committee of the IEEE Industrial Electronics Society, in 2007. In 2014, he has received the Isao Takahashi Power Electronics Award for outstanding achievement in power electronics, and in 2018, the EPE Outstanding Service Award from the European Power Electronics and Drives Association. He is an Associate Editor of the IEEE TRANSACTIONS ON INDUSTRIAL ELECTRONICS, the IEEE TRANSACTIONS ON POWER ELECTRONICS, and the *IET Electric Power Applications*.